Journal of Geoscience and Environment Protection, 2026, 14(2), 36-55
https://www.scirp.org/journal/gep
ISSN Online: 2327-4344
ISSN Print: 2327-4336

Relationship between Convection and Tropical Cyclone Size and Size Change Rate

Praksed Mrosso Rafael[1,2], Ke Peng[1], Yu-Xun Tian[1], Daniel Stephano Semgomba[2], Yiran Liu[1]

[1]School of Atmospheric Sciences, Nanjing University of Information Science & Technology, Nanjing, China
[2]Tanzania Meteorological Authority, Dodoma, Tanzania
Email: praxymrosso@gmail.com

How to cite this paper: Rafael, P. M., Peng, K., Tian, Y.-X., Semgomba, D. S., & Liu, Y. R. (2026). Relationship between Convection and Tropical Cyclone Size and Size Change Rate. *Journal of Geoscience and Environment Protection, 14,* 36-55.
https://doi.org/10.4236/gep.2026.142003

Received: January 6, 2026
Accepted: January 31, 2026
Published: February 3, 2026

Copyright © 2026 by author(s) and Scientific Research Publishing Inc.
This work is licensed under the Creative Commons Attribution International License (CC BY 4.0).
http://creativecommons.org/licenses/by/4.0/
Open Access

Abstract

This study examines the relationship between convection activity and size as well as the size change rate of Tropical Cyclones (TCs) over the Northwestern Pacific Ocean (NWP) from 2001 to 2022. TC size is defined by the radius of 34-kt wind (R34) provided by the Joint Typhoon Warning Center (JTWC) and is classified into small, medium, and large categories across different intensity stages. Deep convection and high clouds were identified using infrared brightness temperature (IR BT) thresholds of <208 K and 208 - 240 K, respectively. Results show that for TCs exceeding Category 1 intensity (>64 knots), convective coverage is proportional to R34, whereas for tropical storms (TS), the relationship is weak. As TC intensity increases, deep convection remains concentrated within the inner core (~100 km from the centre), while convective expansion is driven mainly by the broadening and enhancement of high clouds in the outer core. The TC cases undergoing rapid growth (RG; defined as a 24-hour R34 increase ≥ 83 km) have a significantly smaller R34 than those experiencing slow or no expansion, which is attributed to the higher frequency of RG during the TS stage. The intensity and occurrence ratio of deep convection near R34 are identified as key factors influencing whether TCs undergo RG.

Keywords

TC Size, TC Size Change, Deep Convection, High Clouds

1. Introduction

The North-western Pacific (NWP) is the world's most active basin for tropical cyclones (TCs), accounting for approximately one-third of global TC occurrences (Basconcillo et al., 2021; Yu et al., 2023; Hong & Vinh, 2024). TCs occur throughout the year in this region, with peak activity observed from July to October

(Pandey & Liou, 2020; Yao et al., 2020). The high socioeconomic vulnerability and extensive coastal urbanization in densely populated areas such as China, Japan, and Vietnam significantly amplify the risks posed by landfalling storms (Nguyen et al., 2021; Xu et al., 2024). While past research on TCs primarily focused on their tracks and intensity (Wang et al., 2023; Fu et al., 2024), recent studies highlight that TC size is also a critical factor governing the spatial extent and severity of storm-related disasters (Li et al., 2022; Lin & Wang, 2024; Peng et al., 2024; Wen et al., 2025).

As a closed circulation system organized around deep convection, TC size can be approached from multiple perspectives. Wind-field metrics such as the radius of gale-force winds (R34), 50-knot winds (R50), or 64-knot winds (R64) are commonly used to measure the horizontal extent of TC circulation (Yuan et al., 2023; Wang, 2025). Among these, R34 is the most widely used, as it provides a reliable indicator of storm structure and destructive potential (Chavas et al., 2016; Knaff et al., 2017). Other measures include the radius of the outermost closed isobar (ROCI), which shows the full reach of the TC circulation, and the radius of maximum wind (RMW), which determines the inner-core size and is strongly correlated with storm intensity (Qin et al., 2016; Ruan & Wu, 2022). Alternatively, some studies use convective or precipitation coverage to represent TC size (Lin et al., 2015). Despite the parallel use of wind-field and convective metrics, the quantitative relationship between organized convection, particularly its spatial distribution, and the wind-field structure of TCs remains inadequately understood.

Previous research has identified several environmental processes that modulate outer-core convection and thus influence TC size. For instance, large-scale ocean warming can enhance atmospheric convective instability in outer regions (Sun et al., 2017), while cloud-radiative forcing (CRF) and strengthened planetary boundary-layer (PBL) vertical mixing can promote wider storms by invigorating outer-core convective activity (Bu et al., 2017). Mid-level humidity also plays a key role by sustaining convection in outer rainbands through reduced dry-air entrainment (Hill & Lackmann, 2009). Furthermore, vertical wind shear can induce asymmetric outer-core convection and foster gradual size expansion via enhanced angular momentum transport (Chen et al., 2022). Collectively, these studies suggest that environmental factors affect TC size largely by regulating the organization and persistence of outer-core convection. On the other hand, observational analyses indicate that the most intense convective clouds (IR BT < 208 K) are closely linked to both the frequency and rapid intensification of TCs (e.g., Wu et al., 2020; Peng & Wu, 2020). However, the specific convective signatures, especially the spatial distribution of deep convection relative to the wind field, that correspond to different rates of TC size expansion remain unclear.

This gap motivates the central questions of this study: To what extent does the spatial distribution of convection govern TC size (R34) and its rate of change? More specifically, what convective characteristics, including coverage, intensity, and radial placement, are associated with rapid versus slow expansion of the TC

wind field? Addressing these questions is critical from both scientific and operational perspectives, as improved understanding of the convective drivers of R34 variability can enhance forecasts of wind-field extent, storm-surge zones, and overall hazard footprints.

In this study, we therefore investigate the relationship between organized convection and TC size and size change rate over the NWP. The analysis focuses on quantifying how convective distribution modulates R34 and identifying the convective features linked to different expansion rates. The paper is organized as follows: Section 2 describes the data and methodology. Section 3 describes the influence of convection on TC size. The convective features associated with TC size change rate are described in Section 4. The discussion and conclusion are found in Section 5.

2. Data and Method

NWP Ocean's TC data from 2001 to 2022 were obtained from the International Best Track Archive for Climate Stewardship (IBTrACS, Knapp et al., 2010). The 3-hourly location, maximum wind speed ($V_{\max}$), and radii of gale force wind (R34) were provided by the Joint Typhoon Warning Centre (JTWC). The following criteria are adopted to minimize noise and provide high-quality data: (a) Only records with $V_{\max} \geq 40$ knots are retained; (b) records where R34 exceeds the distance from the TC centre to the nearest coastline are removed; (c) TCs that made landfall during their development stage are entirely discarded. V_{max} is used to represent TC intensity, and the azimuthal mean of R34 across the four quadrants is adopted to characterize TC size. The TC intensity categories used in this study (TS, CAT1-CAT5) are based on the Saffir-Simpson Hurricane Wind Scale (Saffir, 1973; Simpson, 1974). A total of 240 storms during their developing stage (from TS to lifetime maximum intensity) in the NWP were analysed for the period 2001-2022. The 24-hour change in R34 was calculated as $\Delta R34 = R34_{t+24h} - R34_t$. The filtered data set contains 2928 cases of ΔR34 size change throughout the TC lifetime.

The convection is examined using the Infrared Brightness Temperature (IR BT) data from the GridSat-B1 satellite (Knapp et al., 2011), which covers near-global (70˚S - 70˚N, 180˚W - 180˚E) regions with a horizontal resolution of 0.07˚ × 0.07˚ and a temporal interval of three hours. Deep convection and high clouds are defined using thresholds of IR BT < 208 K and 208 < IR BT < 240 K, respectively (Wu & Ruan, 2016).

The fifth-generation reanalysis data from the European Centre for Medium-Range Weather Forecasts (ERA5, Hersbach et al., 2020) were used to calculate the vertical wind shear (VWS) with a horizontal resolution of 0.25˚ × 0.25˚ at 6-hour intervals. VWS was defined as the difference between 850 and 200 hPa, as described in Harnos & Nesbitt (2011).

3. The Distribution of Convection on TC Intensity and Size

TCs were classified as small, medium, and large based on the 33% and 67% per-

centiles, as shown in Table 1, similar to the classification by Lee et al. (2010) within the TS (40 - 63 kt), CAT 1 - 3 (64 - 112 kt), and CAT 4 - 5 (>112 kt) categories. The results show that R34 thresholds vary with TC intensity, whereby the average R34 increases as the TC intensity increases. During the TS stage, small TCs display R34 less than 86 km, while large TCs exceed 116 km. As TCs strengthen to CAT 1 - 3, the thresholds shift upwards, with R34 less than 145 km in small TCs, medium-sized TCs ranging from 145 km to 190 km, and large TCs with R34 above 190 km. Moreover, R34 in the CAT 4 - 5 stage expands further, with R34 less than 207 km in small TCs. Large TCs depict R34 which exceeds 264 km, indicating that as the TC intensifies, its size also tends to expand.

Table 1. The definitions of small, medium, and large TCs (in km) during the TS stage, CAT 1 - 3 stage, and CAT 4 - 5 stage. In brackets (outside brackets) are the R34 size (number of TCs) in each category.

Size/Intensity	Small	Medium	Large
TS	75 [<86.0]	90 [86.0 - 116.0]	75 [>116.0]
CAT [1 - 3]	80 [<145.0]	81 [145.0 - 190.0]	79 [>190.0]
CAT [4 - 5]	46 [<207.0]	50 [207.0 - 269.0]	42 [>269.0]

Figure 1 shows the shear-relative composite of IR BT when the TCs are in different size groups (small, medium, and large) and intensity categories (TS, CAT 1 - 3, and CAT 4 - 5). The results show that the relationship between TC size and convective coverage area varies at different intensities. Thus, as the intensity increases, the convective strength within the typhoon's core intensifies and the convective coverage area expands. During the TS stage (Figures 1(a)-(c)), the convective coverage area is quite similar. Even in small TCs (Figure 1(a)), the coverage area of relatively strong convection (IR <218K) is larger than that in large TCs (Figure 1(c)). CAT 1 - 3 show a large convection coverage area of IR BT <218K in large TCs (Figure 1(f)), although small TCs (Figure 1(d)) show a small coverage area of strong convection IR BT <202K within the core. A large coverage area with strong convection IR BT <202K is observed within the typhoon core in all size groups (Figures 1(h)-(i)). Conversely, R34 during the TS stage exhibits strong convection IR BT <218K across size groups. In contrast, for CAT 1 - 3 and CAT 4 - 5 stages, R34 in larger TCs exhibits convection with IR BT > 218 K.

Generally, the distribution of convection varies with R34 across different intensities, where results revealed a progressive relationship between the radial extent of convection (R_Conv70; defined as the maximum radius of the region where the convective coverage is greater than or equal to 70%) and R34 as the storm intensifies (Figure 2). In the TS stage (Figure 2(a)), the relationship is weak but statistically significant (r = 0.135). In contrast, the CAT 1 - 3 stage (Figure 2(b)) shows a more positive relationship, which is also statistically significant (r = 0.304). As storms intensify, convection expands more systematically

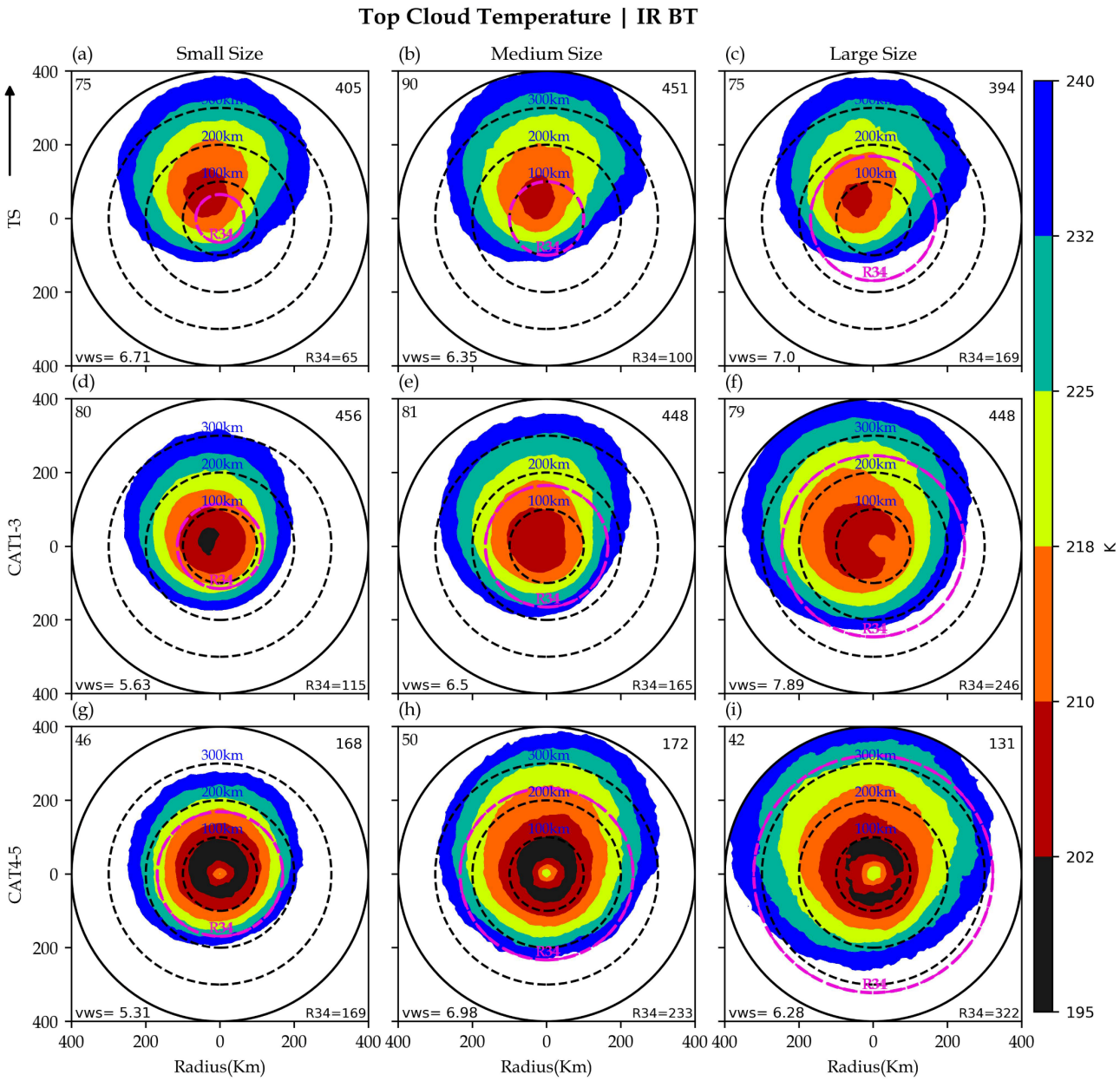

Figure 1. Shear-relative composites of IR BT according to different TC size and intensity categories in the Western North Pacific. The dotted pink circle represents the average R_{34} in each group, and the dotted black circles represent 100 km, 200 km, and 300 km radii from the TC centre. The arrow represents the direction of wind shear. The sample sizes at the top left corner represent the number of TC; at the right corner represent the number of TC cases; the mean vertical wind shear is in the bottom left-hand corner, and the bottom right-hand corner shows the average R34 of each panel.

with the wind field radius. Medium and large TCs increasingly populate the upper right of the scatter, indicating a stronger and more organized convective distribution. In CAT 4 - 5 (**Figure 2(c)**), the relationship improves more significantly ($r = 0.353$). Large TCs exhibit the widest convective radial extent, while small storms remain confined to the lower left region. Generally, the result indicates that during the early stages of TC development, the extent of convective coverage shows limited correlation with the wind profile of the vortex. Therefore, the size of

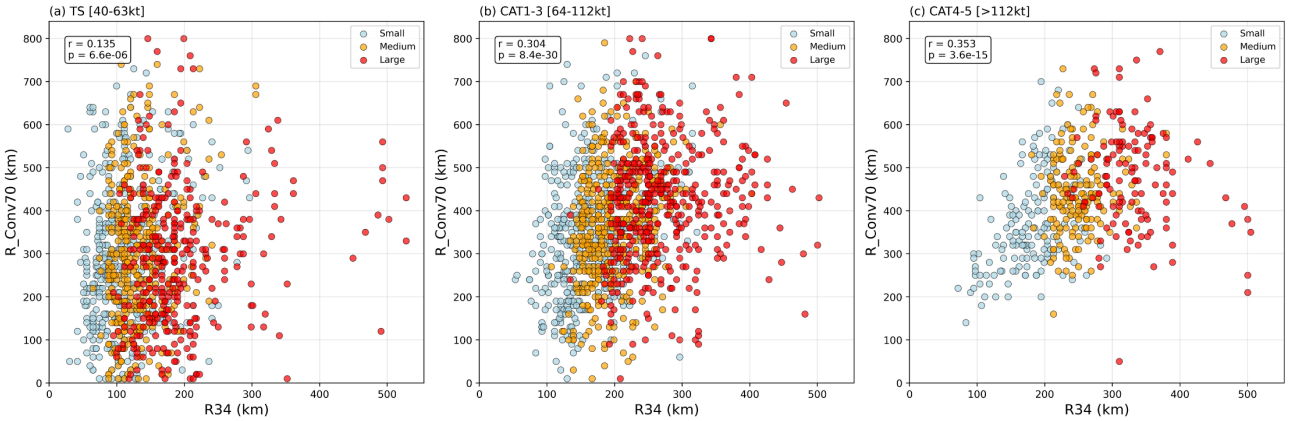

Figure 2. The relationship between tropical cyclone size (R34) and the radial extent of convection (BT < 240 K) (R_Conv70) for (a) TS, (b) CAT 1 - 3, and (c) CAT 4 - 5 in the western North Pacific. Light blue, brown, and red colours represent small, medium, and large TCs, respectively. The Pearson correlation coefficient (r) and corresponding p-value indicate the strength and statistical significance of the relationship in each intensity category.

convective coverage does not necessarily reflect the scale of the TC vortex. However, as the TC intensifies, the extent of convective coverage increasingly represents the scale of the vortex.

The characteristics of deep convective clouds in relation to TC size and intensity are examined in **Figure 3**, which presents the occurrence frequency of deep convection across different intensities. The occurrence frequency of deep convection is calculated as the number of samples where deep convection occurs (BT < 208 K) per grid point divided by the total number of samples. Across all intensity categories, the occurrence frequency of deep convection is less than 70% confined within 100 km. However, the occurrence frequency increases as the storms intensify. CAT 4 - 5 exhibits a high rate of deep convection of more than 70% compared to other categories, although CAT 1 - 3 is the second highest.

On the other hand, in large TCs (**Figure 3(c)**), the occurrence frequency around R34 was less than 50%, whereas for small and medium TCs, it was less than 70% and 60%, respectively. This indicates that for large TCs, the locations where deep convection occurs are more scattered. During CAT 1 - 3 (**Figures 3(d)-(f)**), the occurrence frequency near R34 for small, medium, and large was 50%, 40%, and 30%, respectively. Conversely, R34 around CAT 4 - 5 (**Figures 3(g)-(i)**) shows a very low percentage of deep convection.

Conversely, **Figure 4** presents the shear-relative frequency distribution of high clouds, which shows that the occurrence frequency rate of high clouds in the inner core is lower for all TC categories due to the high-frequency occurrence of deep convection in the inner core (**Figure 3**). During the TS stage, the occurrence frequency of high clouds around R34 for small TCs was 40%, while medium and large TCs were less than 50%. A high occurrence frequency of high clouds, about 50% to 70%, appears around R34 in CAT 1 - 3 (**Figure 4(f)**). The highest convection rate, which is greater than 60%, occurs near R34 in CAT 4 - 5, especially in medium and large TC (**Figures 4(h)-(i)**). Generally, during CAT 1 - 3 and CAT

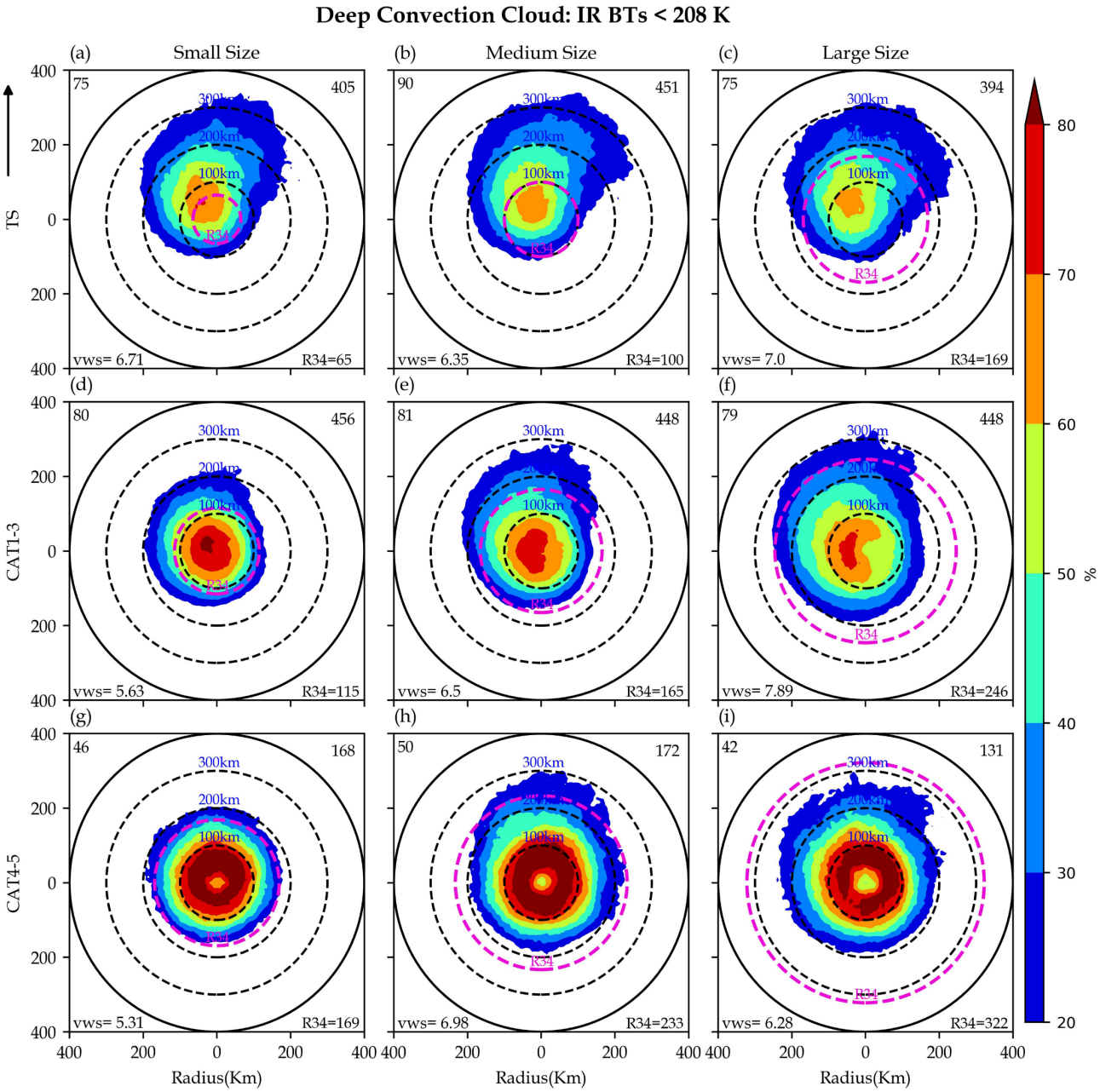

Figure 3. Shear-relative composites of deep convective clouds with IR BT < 208 K percentage coverage for different TC size and intensity categories in the western North Pacific. The dotted pink circle represents the average R34 in each group, and the dotted black circles represent 100 km, 200 km, and 300 km radii from the TC centre. The arrow represents the direction of wind shear. The sample sizes at the top left corner represent the number of TCs, at the right corner represent the number of TC cases, the mean vertical wind shear is shown in the bottom left corner, and the bottom right corner shows the average R34 of each panel.

4 - 5 TCs, the locations with a higher occurrence frequency of high clouds appear to be relatively close to the R34. As the TC intensity increases, the radius encompassing high-frequency high clouds also expands, indicating an increase in the typhoon's convective cloud coverage. This finding aligns with the results presented in Figure 1 and Figure 2.

In summary, across all size and intensity categories, the results show that

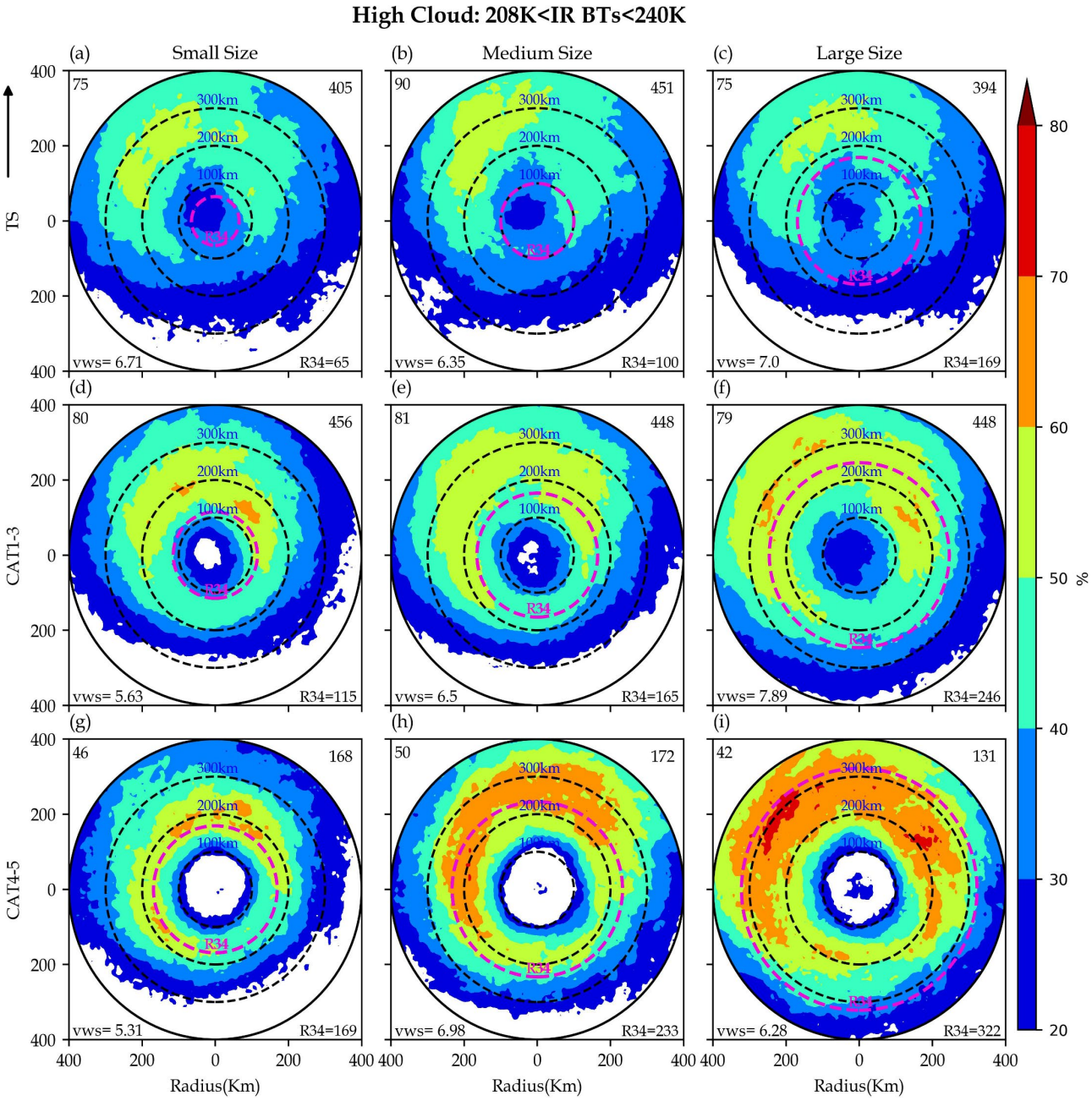

Figure 4. Same as **Figure 3**, but the colours show the occurrence frequency for BT of very high clouds.

convection distribution systematically expands and reorganizes as storms intensify, influencing the R34 size. The study also found that, during the TS stage, the relationship between convective coverage area and vortex size is relatively weak, suggesting that the size of convective coverage does not necessarily reflect the scale of the TC vortex. However, as the TC intensifies, the extent of convective coverage increasingly represents the scale of the vortex. Additionally, the occurrence frequency of high clouds appears to be relatively close to the R34. As the TC intensity increases, the radius encompassing a high frequency of high clouds also expands, indicating an increase in the typhoon's convective cloud coverage.

4. Convective Characteristics at Different TC Size Expansion Rates

The expansion rate of TC size is another key aspect examined in this study, as earlier work has demonstrated that convective characteristics exert a significant influence on typhoon development (Hong & Wu, 2023). We classify 24-h ΔR34 into non-growth (NG; $\Delta R_{34} \leq 0$ km), slow growth (SG; $0 < \Delta R_{34} < 83$ km), and rapid growth (RG). RG occurs when R34 increases by ≥83 km within 24 hours, representing the 90th percentile of R34 growth changes as defined by Li et al. (2022). The frequency and cumulative distribution functions are presented in **Figure 5**. Values within the range [bin-10, bin+10] are grouped in each bin. The cumulative frequency distributions show that the 90th percentile of ΔR34 in all cases is 83 km. Therefore, in this study, the criteria for RG rate were defined as $\Delta R34_{24h} \geq 83$ km.

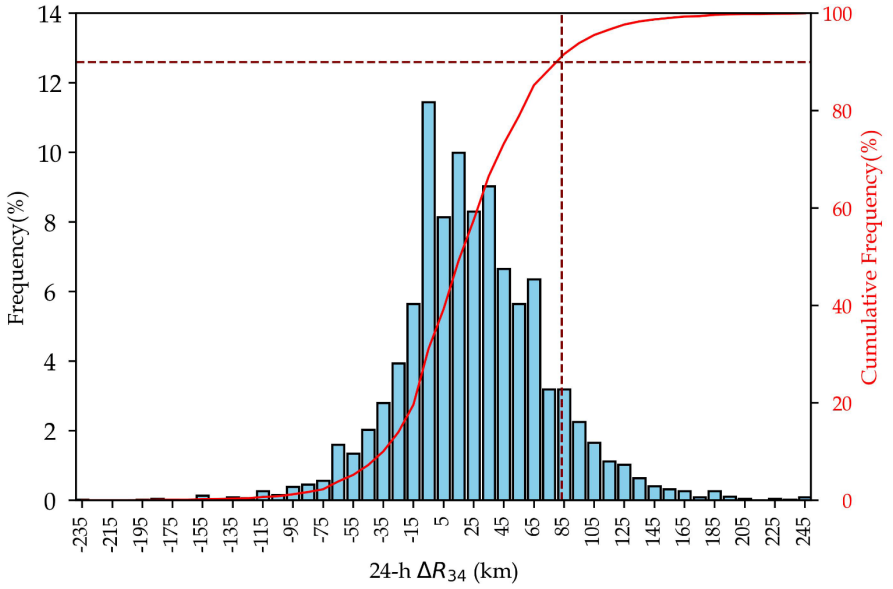

Figure 5. The frequency and cumulative frequency distributions of 24-hΔR_{34} (km). The dotted line defines the 90th percentile, which is the threshold for RG.

The convection distribution for the R34 change rate with the intensity (**Figure 6**) shows that colder IR BT is concentrated within 100 km (**Figures 6(a)-(c)**), and the convection coverage area increases during RG (**Figure 6(c)**). NG storms show a weaker convective distribution around 300 km and more compact convection within or close to the inner core (**Figure 6(a)**), with IR BT of less than 227 K around R34. Convection in the SG (**Figure 6(b)**) exhibits an intermediate structure, with convective bands extending moderately outward with IR BT of less than 220 K within R34 compared to NG. However, RG (**Figure 6(c)**) shows a wider spread of colder IR BT with a temperature less than 227 K within 300 km and less than 213 K within R34. Additionally, deep convective clouds with colder IR BT in NG R34 (**Figure 6(d)**) are concentrated within 100 km of the inner core with IR BT less than 197 K, and less than 200 K within R34. In contrast, near R34,

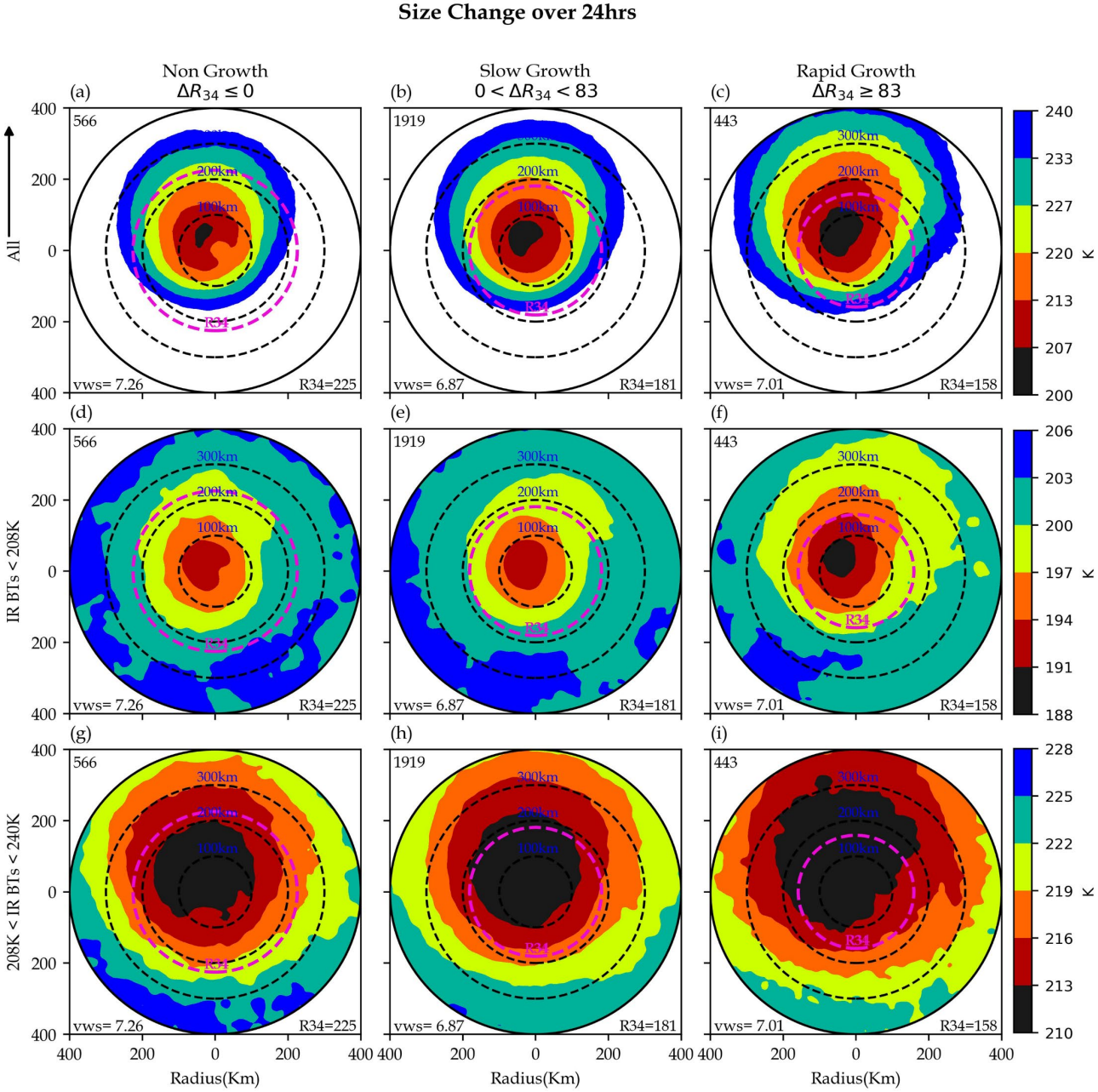

Figure 6. Shear-relative composites of IR BT according to different TC size changes and convective features (deep and high clouds) in the Western North Pacific. The dotted pink circle represents the average R34 in each group, and the dotted black circles represent 100 km, 200 km, and 300 km radii from the TC centre. The arrow represents the direction of wind shear. The sample sizes in the top left corner represent the number of TC cases, the mean vertical wind shear in the bottom left corner, and the bottom right corner shows the average R34 of each panel.

IR BT less than 194 K was observed in RG (**Figure 6(f)**). The high cloud convection displays a wider distribution, with lower IR BT of less than 213 K within 100 km, extending outward with IR BT less than 216 K in NG and beyond R34 (**Figure 6(g)**). Conversely, SG storms show deep convection concentrated in the inner core, with high clouds and moderate convective distribution extending beyond R34, with IR BT below 213 K. For RG (**Figure 6(i)**), high clouds exhibit more

widespread lower IR BT extending beyond R34 with IR BT less than 213 K within 200 km and beyond R34.

There is a notable decrease in the average R34 from 225 km in the NG group to 181 km in the SG group and 158 km in the RG group (Figure 6). Specifically, among the 443 RG cases, 247 (56%) occur during the TS stage (Table 2), indicating that TS cases constitute the majority of the RG storms. Because TCs are climatologically smaller during the TS stage (Table 1), the dominance of TS cases leads to a smaller mean R34 for the RG group.

As storm intensity increases to CAT 1 - 3, the number of RG cases decreases to 164, with a substantial fraction occurring in medium and large sized storms (59 and 68 cases, respectively). In the CAT 4 - 5 stage, RG becomes relatively rare, with only 32 cases, mainly in medium and large TCs (12 and 14 cases, respectively). These results are further supported by Figure 7, which shows that RG

Table 2. The distribution ratio of 24-h size change for 443 RG cases according to size and intensity categories. The ratios of RG cases for each size and intensity are provided. The total number of RG cases and the percentage of the RG sample total contributed by each of the size classes are also presented.

Size/intensity	Small	Medium	Large	All
TS	108	98	41	247
CAT [1 - 3]	37	59	68	164
CAT [4 - 5]	6	12	14	32
Total Cases [%]	151 [34.09]	169 [38.15]	123 [27.77]	443 [100.0]

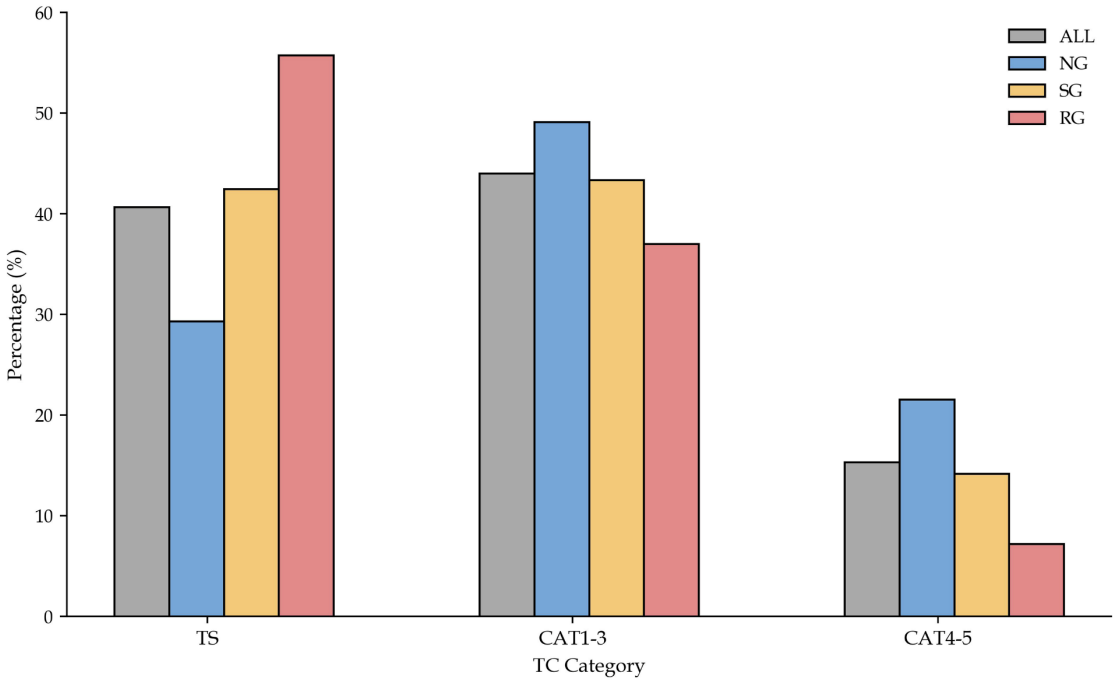

Figure 7. The percentage distribution ratio of 24-h size change for all cases, NG, SG, and RG cases according to intensity categories.

accounts for the largest proportion of approximately 58% during the TS stage. In comparison, SG represents about 42% of cases, while NG storms are the least frequent at this stage. As storms intensify to the CAT 1 - 3 stage, the proportional shifts, with NG exhibiting about 49%, followed by SG (43%) and RG (37%). The trend becomes more pronounced at the CAT 4 - 5 stage, where NG dominates approximately 21%, whereas SG and RG account for only about 14% and 7% respectively, confirming that rapid size expansion is most prevalent during the early and relatively weak stages of TC development.

Figure 8 presents the shear-relative frequency distribution of very deep convective clouds with respect to TC size change and intensity. Results show that there is a high percentage of deep convection within 100 km, and the percentage increases as the storm intensifies. For TS, the occurrence rate of deep convection is less than 70% concentrated within 100 km. However, in NG and SG storms (**Figure 8(a)** & **Figure 8(b)**), the occurrence ratio around R34 was less than 30%, and during RG storms, the occurrence ratio was less than 50%. For CAT 1 - 3, the higher occurrence rate of deep convection is confined within 100 km. For NG and SG (**Figure 8(d)** & **Figure 8(e)**), the occurrence of deep convection was around 20%, and RG was less than 50% near R34. The occurrence rate of very deep convection in the inner core is significantly higher in CAT 4 - 5 than in other categories, which is greater than 70% within 100 km, with a very low percentage ratio of deep convection (**Figures 8(g)-(i)**) around R34. However, the occurrence rate of very deep convection in the inner core for the CAT 1 - 3 category is the second highest.

However, the occurrence rate of high clouds in the inner core is lower for all TC size change categories (**Figure 9**) due to the high occurrence rates of deep convection in the inner core. During the TS, the occurrence ratio of high clouds around R34 for NG storms (**Figure 9(a)**) was between 40% and 50%, while SG and RG storms (**Figure 9(b)** & **Figure 9(c)**) were between 30% and 50%. A high occurrence ratio of high clouds, about 60% to 70%, appears around R34 in CAT 1 - 3 (**Figure 9(f)**). The highest high clouds occurrence ratio, which is around 70%, occurs near and beyond R34 in CAT 4 - 5, especially in RG storms (**Figure 9(h)** & **Figure 9(i)**). This implies that as the TC intensifies, the high clouds convection concentrates more in the outer core region.

Figure 10 presents differences in R34 (on the left) and convection distribution within $0.8R34 \le R34 \le 1.2R34$ annulus (on the right). In both the TS and CAT 1 - 3 stages, RG storms exhibit the smallest R34, with median and mean values that are significantly lower than those of NG and SG storms. This indicates that storms that undergo RG generally begin from smaller sizes and weaker intensities, as it was also shown in Table 2 that most of the RG cases were observed during the TS stage and small size group. Conversely, R34 across NG, SG, and RG during the CAT 4 - 5 stage overlap substantially and are mostly not significant.

On the other hand, the IR BT distributions show a relationship with size change across all intensity categories. RG storms display the coldest IR BT values within

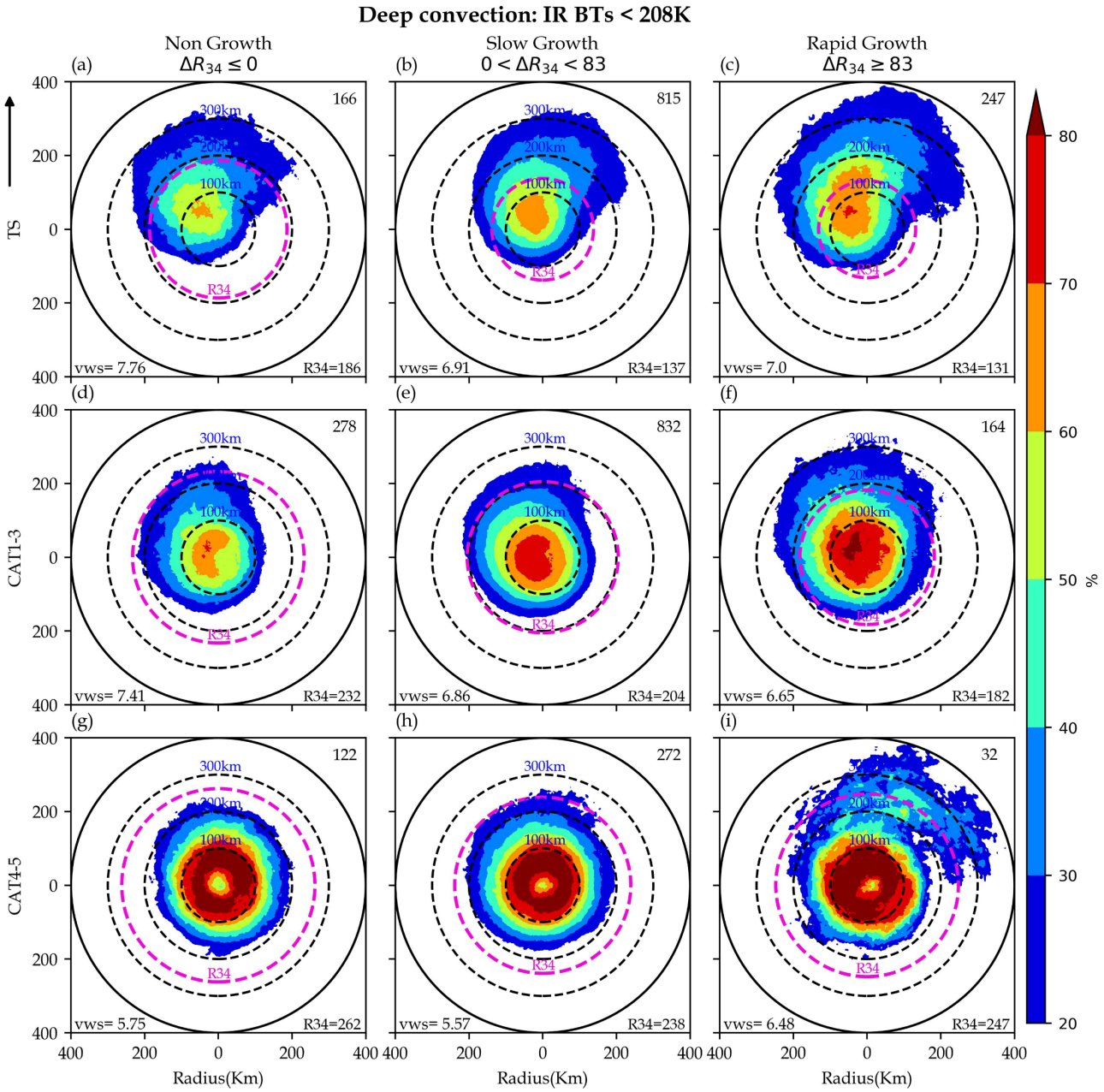

Figure 8. Shear-relative composites of deep convective clouds with IR BT<208K percentage coverage for TC size change and intensity categories in the western North Pacific. The dotted pink circle represents the average R34 in each group, and the dotted black circles represent 100 km, 200 km, and 300 km radii from the TC centre. The arrow represents the direction of wind shear. The number of cases is shown at the top right corner, the mean vertical wind shear is shown in the bottom left corner, and the bottom right corner shows the average R34 of each panel.

the $0.8R34 \leq R34 \leq 1.2R34$ annulus, indicating the presence of deeper convection distributed near R34, while NG storms exhibit the warmest BT values, reflecting weaker convective activity near R34. These results imply that enhanced convection surrounding the R34 region, especially in RG, is strongly associated with 24 h size expansion.

The distribution ratio for deep and high clouds within the $0.8R34 \leq R34 \leq 1.2R34$

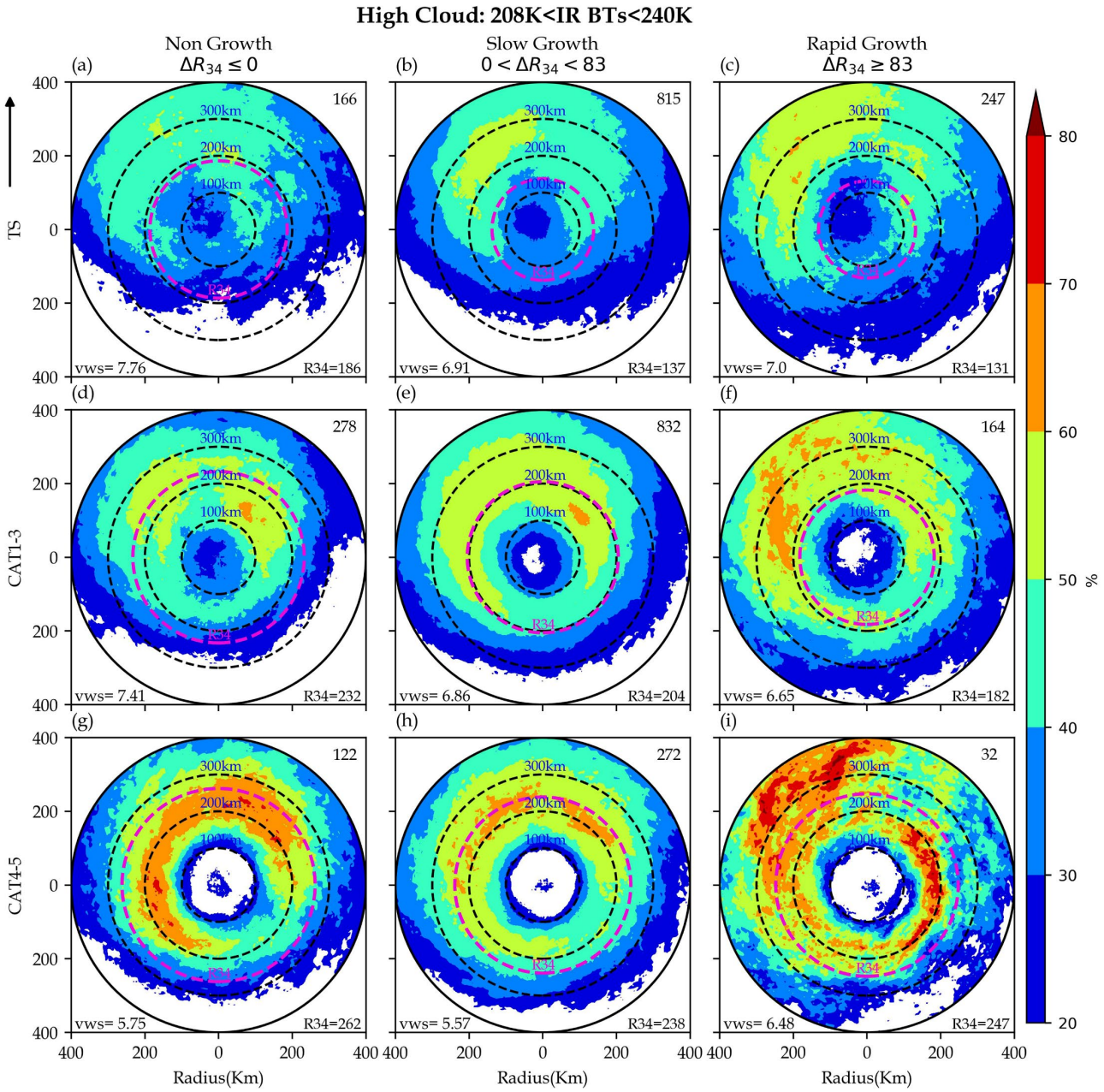

Figure 9. Same as **Figure 8**, but the colours show the occurrence frequency for BT of very high clouds.

annulus is shown in **Figure 11**. The results reveal that RG storms exhibit the highest ratios of deep convection within the annulus for all intensity categories (**Figure 11(a)**, **Figure 11(c)**, **Figure 11(f)**). Across all intensity categories, RG display a higher deep convection ratio than both SG and NG storms, with all pairwise differences statistically significant. In contrast, the high clouds (**Figure 11(b)**, **Figure 11(d)**, **Figure 11(f)**) reveal that although RG storms show a higher high clouds ratio in the TS stage, NG storms show the highest high cloud ratio, indicating that high clouds alone do not distinguish growth categories as clearly as deep convection.

In summary, R34 change over 24 h (NG, SG, and RG) is strongly associated

with the structure and distribution of convection, particularly during RG. The convection distribution showed colder and widespread IR BT becoming increasingly dominant as storms shift from NG to RG, but RG storms show widespread colder IR BT. The occurrence ratio of deep convective clouds is especially concentrated within 100 km, and the percentage of occurrence increases with intensity.

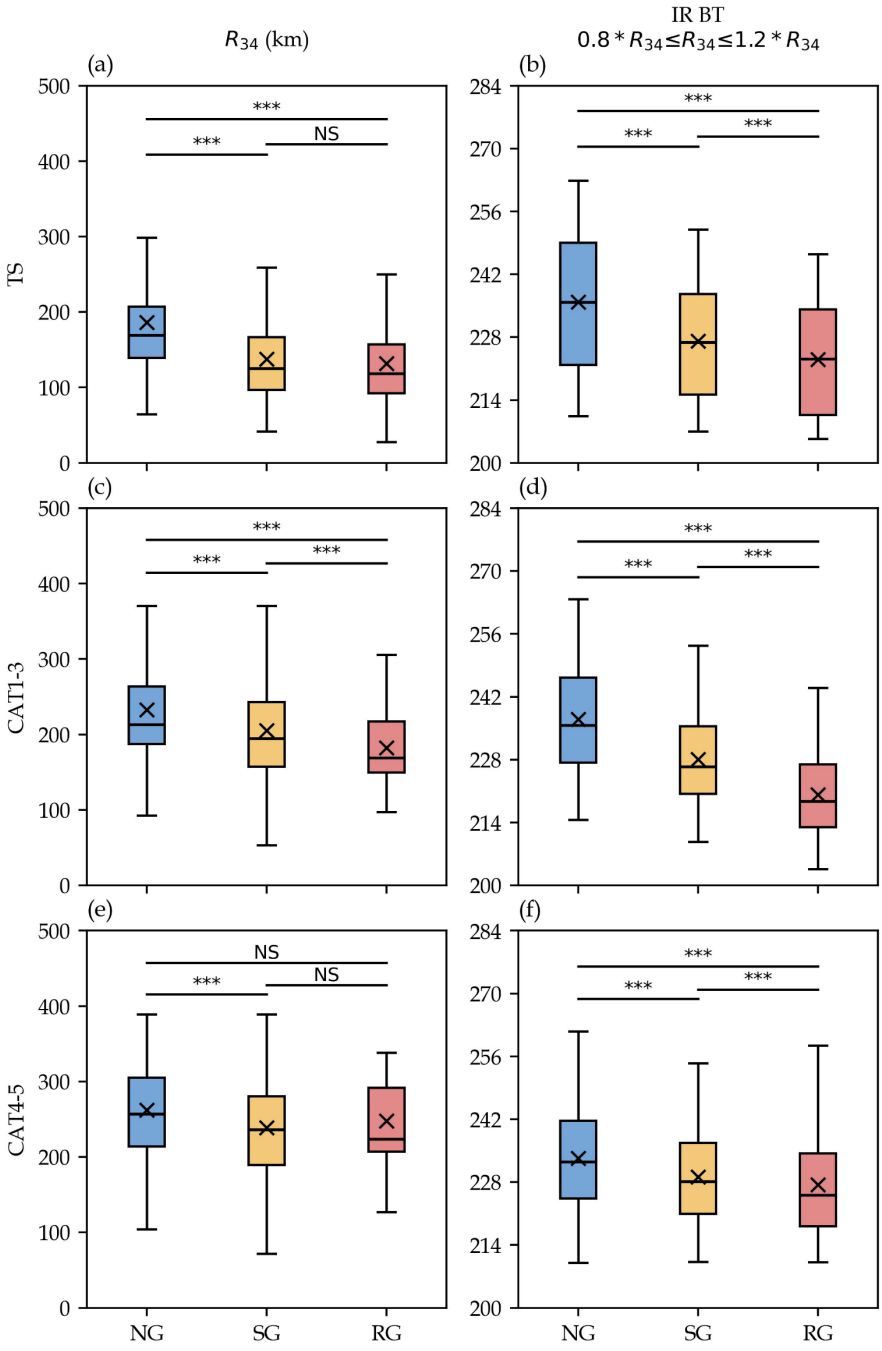

Figure 10. Box plot for R34 (left side) and IR BT within $0.8R34 \leq R34 \leq 1.2R34$ annulus (right side) across 24 h size change (NG, SG, and RG) and intensity categories (TS, CAT 1 - 3, and CAT 4 - 5). Boxes show the interquartile range with median and mean (x); *** indicates statistical significance $p < 0.05$, and NS indicates not significant.

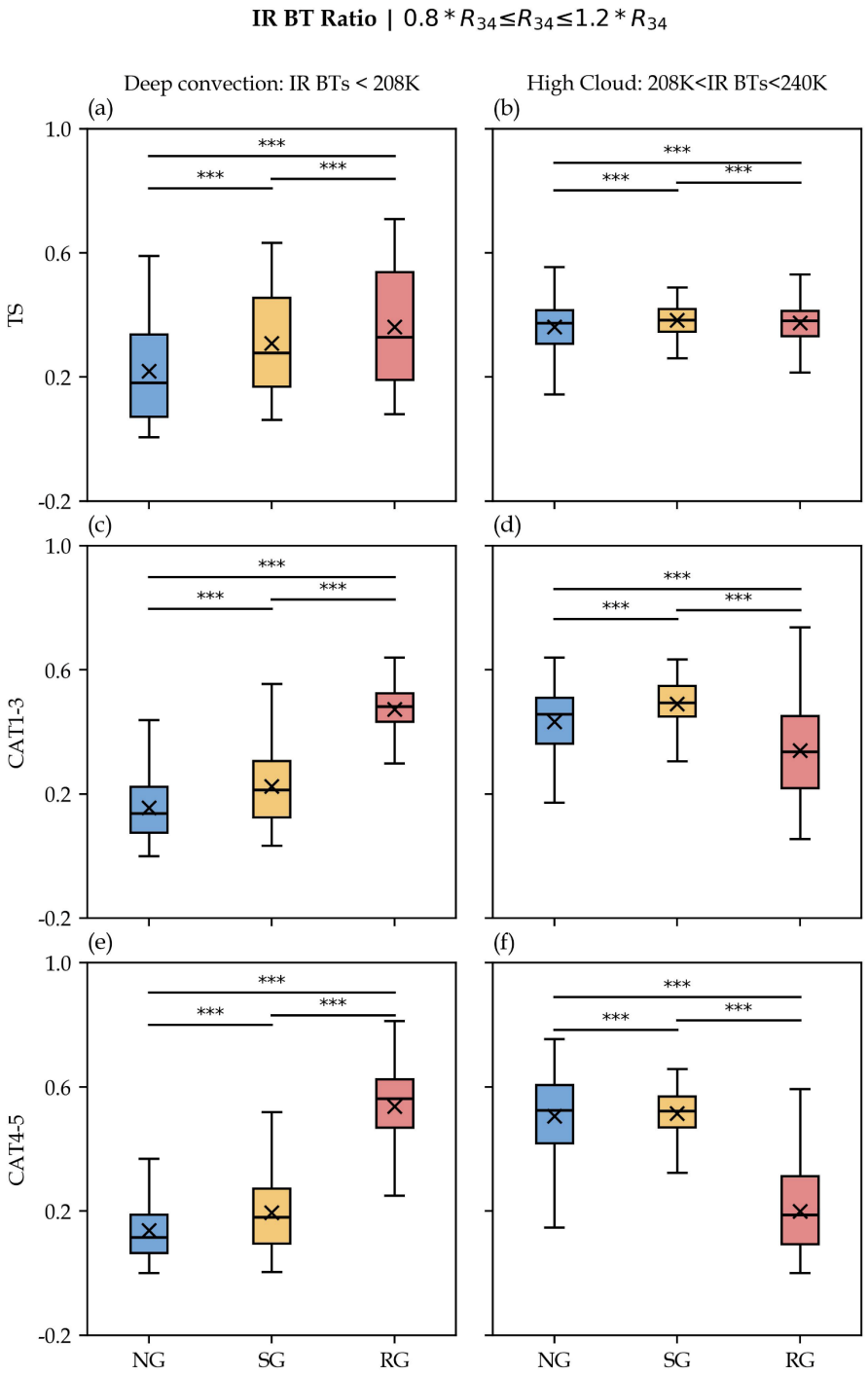

Figure 11. Box plot for deep convective clouds (left side) and high clouds (right side) ratio within $0.8R34 \leq R34 \leq 1.2R34$ annulus across 24 h size change (NG, SG, and RG) and intensity categories (TS, CAT 1 - 3, and CAT 4 - 5). Boxes show the interquartile range with medians and mean (x), *** indicates statistical significance ($p < 0.05$), and NS indicates not significant.

In contrast, the high percentage occurrence ratio of high clouds extends more outward and becomes more dominant in the CAT5 4-5 stage, particularly near R34. On the other hand, provided RG showed a wider spread of colder IR BT

compared to NG and SG, its overall R34 size is the smallest. This is because the high percentage of RG cases was observed during TS and in small sizes, which makes the overall average R34 size smaller than that of NG and SG. The result confirms RG exhibits the significantly smallest average R34 as well as colder IR BT within $0.8R34 \le R34 \le 1.2R34$ compared to NG and SG. This confirms that the lower IR BT near R34 is a key driver of RG expansion.

5. Discussion and Conclusion

This study aims to examine the relationship between convection and TC size (R34) and size change. As TC intensity increases, the convective strength within the TCs' inner core intensifies and the convective coverage area expands. During the TS stage, the correlation between convective coverage and R34 is relatively weak. As storms intensify into CAT 1 - 3 and CAT 4 - 5 stages, the relationship becomes significantly stronger, with more expansive convective coverage. The percentage ratio for deep convection and high clouds further shows that a high percentage ratio of deep convection with colder IR BT occurs within 200 km and near R34 in most of the size groups during TS and CAT 1 - 3, but far from R34, especially during CAT 4 - 5 in large TC, whereas a high clouds percentage ratio with colder IR BT occurs beyond 200 km and around R34.

Additionally, TC size change rate (NG, SG, and RG) revealed a connection between convection and 24 h R34 size change. The results depict that RG cases tend to occur when TCs are weaker and small in size. The result is in line with the study by Li et al. (2023), which also found R34 size change tends to increase more rapidly when the initial R34 is smaller. TC size growth is associated with high coverage of deep convective clouds (Hong & Wu, 2023). Heating associated with convection in the outer vortex enhances the inward flux of absolute angular momentum through the boundary layer, which contributes to the growth of the storm's outer size (Chan & Chan, 2013; Tsuji et al., 2016). RG storms show a higher percentage ratio of deep convection than high clouds within the $0.8R34 \le R34 \le 1.2R34$ annulus, indicating strong outer core convective activity that enhances low-level angular momentum transport through convective heating near the R34 radius and promotes the expansion of R34. This result is consistent with the prior study by Ruan & Wu (2022), which found that as the TC intensifies, R34 expands rapidly when very deep convective clouds occur in both the inner and outer regions. Even though the high clouds occurrence ratio increases with intensity, it does not distinguish R34 size change as clearly as deep convection, emphasizing that deep convective distribution within $0.8R34 \le R34 \le 1.2R34$ annulus is the dominant driver of 24-h R34 expansion.

In general, this study concludes that convection is a crucial factor for R34 evolution over NWP. Deep convection distribution near R34 strongly favors RG growth. Although high clouds become increasingly dominant in the outer core as storms intensify, they are not reliable indicators of size change on their own. Instead, deep convective distribution near the R34 appears to be the most consistent

and physically predictive of 24-h TC size change. These findings will provide important insights for improving operational forecasts of TC wind field structure and evolution, especially during early stages when RG changes are most likely.

Conflicts of Interest

The authors declare no conflicts of interest regarding the publication of this paper.

References

Basconcillo, J., Cha, E. J., & Moon, I. J. (2021). Characterizing the Highest Tropical Cyclone Frequency in the Western North Pacific Since 1984. *Scientific Reports*, *11*, Article No. 14350. https://doi.org/10.1038/s41598-021-93824-2

Bu, Y. P., Fovell, R. G., & Corbosiero, K. L. (2017). The Influences of Boundary Layer Mixing and Cloud-Radiative Forcing on Tropical Cyclone Size. *Journal of the Atmospheric Sciences, 74,* 1273-1292. https://doi.org/10.1175/jas-d-16-0231.1

Chan, K. T. F., & Chan, J. C. L. (2013). Angular Momentum Transports and Synoptic Flow Patterns Associated with Tropical Cyclone Size Change. *Monthly Weather Review, 141,* 3985-4007. https://doi.org/10.1175/mwr-d-12-00204.1

Chavas, D. R., Lin, N., Dong, W., & Lin, Y. (2016). Observed Tropical Cyclone Size Revisited. *Journal of Climate, 29,* 2923-2939. https://doi.org/10.1175/jcli-d-15-0731.1

Chen, K., Chen, G., & Shi, D. (2022). Reexamination of the Relationship between Tropical Cyclone Size and Intensity over the Western North Pacific. *Advances in Atmospheric Sciences, 39,* 1956-1968. https://doi.org/10.1007/s00376-022-1450-6

Fu, K. J., Guo, Y., & Tan, Z. (2024). Long-Term Trend of the Tropical Cyclone Translation Speed over the Western North Pacific with Track Change. *Climate Dynamics, 63,* Article No. 45. https://doi.org/10.1007/s00382-024-07510-w

Harnos, D. S., & Nesbitt, S. W. (2011). Convective Structure in Rapidly Intensifying Tropical Cyclones as Depicted by Passive Microwave Measurements. *Geophysical Research Letters, 38,* L07805. https://doi.org/10.1029/2011gl047010

Hersbach, H., Bell, B., Berrisford, P., Hirahara, S., Horányi, A., Muñoz-Sabater, J. et al. (2020). The ERA5 Global Reanalysis. *Quarterly Journal of the Royal Meteorological Society, 146,* 1999-2049. https://doi.org/10.1002/qj.3803

Hill, K. A., & Lackmann, G. M. (2009). Influence of Environmental Humidity on Tropical Cyclone Size. *Monthly Weather Review, 137,* 3294-3315. https://doi.org/10.1175/2009mwr2679.1

Hong, D. T. B., & Vinh, T. Q. (2024). Modeling Seasonal Typhoon Genesis in the Northwest Pacific Using Probabilistic Approaches. *Modeling Earth Systems and Environment, 10,* 5891-5906. https://doi.org/10.1007/s40808-024-02122-z

Hong, J., & Wu, Q. (2023). Diurnal Variations of Tropical Cyclone Outer Region Size Growth. *Atmospheric Science Letters, 24,* e1183. https://doi.org/10.1002/asl.1183

Knaff, J. A., Sampson, C. R., & Chirokova, G. (2017). A Global Statistical-Dynamical Tropical Cyclone Wind Radii Forecast Scheme. *Weather and Forecasting, 32,* 629-644. https://doi.org/10.1175/waf-d-16-0168.1

Knapp, K. R., Ansari, S., Bain, C. L., Bourassa, M. A., Dickinson, M. J., Funk, C. et al. (2011). Globally Gridded Satellite Observations for Climate Studies. *Bulletin of the American Meteorological Society, 92,* 893-907. https://doi.org/10.1175/2011bams3039.1

Knapp, K. R., Kruk, M. C., Levinson, D. H., Diamond, H. J., & Neumann, C. J. (2010). The International Best Track Archive for Climate Stewardship (IBTrACS): Unifying Tropical

Cyclone Data. *Bulletin of the American Meteorological Society, 91,* 363-376. https://doi.org/10.1175/2009bams2755.1

Lee, C. S., Cheung, K. K. W., Fang, W. T., & Elsberry, R. L. (2010). Initial Maintenance of Tropical Cyclone Size in the Western North Pacific. *Monthly Weather Review, 138,* 3207-3223. https://doi.org/10.1175/2010mwr3023.1

Li, Y., Tang, Y., & Wang, S. (2022). Rapid Growth of Outer Size of Tropical Cyclones: A New Perspective on Their Destructive Potential. *Geophysical Research Letters, 49,* e2022GL099230. https://doi.org/10.1029/2022gl099230

Li, Y., Tang, Y., Wang, S., & Li, X. (2023). Rapid Growth of Tropical Cyclone Outer Size over the Western North Pacific. *Remote Sensing, 15,* Article No. 486. https://doi.org/10.3390/rs15020486

Lin, P., & Wang, N. (2024). A Data-Driven Approach for Regional-Scale Fine-Resolution Disaster Impact Prediction under Tropical Cyclones. *Natural Hazards, 120,* 7461-7479. https://doi.org/10.1007/s11069-024-06527-y

Lin, Y., Zhao, M., & Zhang, M. (2015). Tropical Cyclone Rainfall Area Controlled by Relative Sea Surface Temperature. *Nature Communications, 6,* Article No. 6591. https://doi.org/10.1038/ncomms7591

Nguyen, C. H., Dang, K. B., Ngo, V. L., Dang, V. B., Truong, Q. H., Nguyen, D. H. et al. (2021). New Approach to Assess Multi-Scale Coastal Landscape Vulnerability to Erosion in Tropical Storms in Vietnam. *Sustainability, 13,* Article No. 1004. https://doi.org/10.3390/su13021004

Pandey, R. S., & Liou, Y. A. (2020). Decadal Behaviors of Tropical Storm Tracks in the Northwest Pacific Ocean. *Atmospheric Research, 246,* Article ID: 105143. https://doi.org/10.1016/j.atmosres.2020.105143

Peng, C. H., & Wu, C. C. (2020). The Impact of Outer-Core Surface Heat Fluxes on the Convective Activities and Rapid Intensification of Tropical Cyclones. *Journal of the Atmospheric Sciences, 77,* 3907-3927. https://doi.org/10.1175/jas-d-19-0348.1

Peng, K., Tian, Y. X., Fang, J., Liu, Y., & Gu, J. F. (2024). Diversity of Tropical Cyclones Rapid Intensification. *Geophysical Research Letters, 51,* e2023GL108006. https://doi.org/10.1029/2023gl108006

Qin, N., Zhang, D. L., & Li, Y. (2016). A Statistical Analysis of Steady Eyewall Sizes Associated with Rapidly Intensifying Hurricanes. *Weather and Forecasting, 31,* 737-742. https://doi.org/10.1175/waf-d-16-0016.1

Ruan, Z., & Wu, Q. (2022a). Relationship between Size and Intensity in North Atlantic Tropical Cyclones with Steady Radii of Maximum Wind. *Geophysical Research Letters, 49,* e2021GL095632. https://doi.org/10.1029/2021gl095632

Saffir, H. S. (1973). Hurricane Wind and Storm Surge. *The Military Engineer, 65,* 4-5.

Simpson, R. H. (1974). The Hurricane Disaster-Potential Scale. *Weatherwise, 27,* 169-186.

Sun, Y., Zhong, Z., Li, T., Yi, L., Hu, Y., Wan, H. et al. (2017). Impact of Ocean Warming on Tropical Cyclone Size and Its Destructiveness. *Scientific Reports, 7,* Article No. 8154. https://doi.org/10.1038/s41598-017-08533-6

Tsuji, H., Itoh, H., & Nakajima, K. (2016). Mechanism Governing the Size Change of Tropical Cyclone-Like Vortices. *Journal of the Meteorological Society of Japan. Ser. II, 94,* 219-236. https://doi.org/10.2151/jmsj.2016-012

Wang, C. (2025). Physics-Enhanced Tropical Cyclone Network for Size Estimation. In *2025 5th International Conference on Artificial Intelligence and Industrial Technology Applications, AIITA 2025* (pp. 1209-1212). IEEE.

Wang, L., Wan, B., Zhou, S., Sun, H., & Gao, Z. (2023). Forecasting Tropical Cyclone Tracks in the Northwestern Pacific Based on a Deep-Learning Model. *Geoscientific Model Development, 16,* 2167-2179. https://doi.org/10.5194/gmd-16-2167-2023

Wen, S., Fang, G., Zhao, L., Ge, Y., & Chen, X. (2025). Estimation of Tropical Cyclone-Induced Wind, Rainfall, and Wave Multihazards for Selected Coastal Cities in China. *Journal of Structural Engineering, 151,* Article ID: 04025039. https://doi.org/10.1061/jsendh.steng-14067

Wu, Q., & Ruan, Z. (2016). Diurnal Variations of the Areas and Temperatures in Tropical Cyclone Clouds. *Quarterly Journal of the Royal Meteorological Society, 142,* 2788-2796. https://doi.org/10.1002/qj.2868

Wu, Q., Hong, J., & Ruan, Z. (2020). Diurnal Variations in Tropical Cyclone Intensification. *Geophysical Research Letters, 47,* e2020GL090397. https://doi.org/10.1029/2020gl090397

Xu, H., Hou, X., Pan, S., Bray, M., & Wang, C. (2024). Socioeconomic Impacts from Coastal Flooding in the 21st Century China's Coastal Zone: A Coupling Analysis between Coastal Flood Risk and Socioeconomic Development. *Science of the Total Environment, 917,* Article ID: 170187. https://doi.org/10.1016/j.scitotenv.2024.170187

Yao, X., Zhao, D., & Li, Y. (2020). Autumn Tropical Cyclones over the Western North Pacific during 1949-2016: A Statistical Study. *Journal of Meteorological Research, 34,* 150-162. https://doi.org/10.1007/s13351-020-9019-8

Yu, J., Zhang, H., Wang, H., Tian, D., & Li, J. (2023). Upper-Ocean Structure Variability in the Northwest Pacific Ocean in Response to Tropical Cyclones. *Frontiers in Marine Science, 10,* Article ID: 1245348. https://doi.org/10.3389/fmars.2023.1245348

Yuan, S., You, Q., Mu, B., Qin, B., & Xu, J. (2023). Estimating the Tropical Cyclone Wind Structure Using Physics-Incorporated Networks. *Frontiers in Earth Science, 10,* Article ID: 1024979. https://doi.org/10.3389/feart.2022.1024979